

New Physics at Neutron Beam Dump

P. S. Bhupal Dev,^{1,*} Bhaskar Dutta,^{2,†} Tao Han,^{3,‡} Aparajitha Karthikeyan,^{2,§} Doojin Kim,^{2,¶} and Hyunyong Kim^{2,**}

¹*Department of Physics and McDonnell Center for the Space Sciences, Washington University, St. Louis, MO 63130, USA*

²*Mitchell Institute for Fundamental Physics and Astronomy, Department of Physics and Astronomy, Texas A&M University, College Station, TX 77843, USA*

³*PITT PACC, Department of Physics and Astronomy, University of Pittsburgh, Pittsburgh, PA 15260, USA*

We find a new utility of neutrons, usually treated as an experimental nuisance causing unwanted background, in probing new physics signals. They can either be radiated from neutrons (neutron bremsstrahlung) or appear through secondary particles from neutron-on-target interactions, dubbed “neutron beam dump”. As a concrete example, we take the FASER/FASER2 experiment as a “factory” of high-energy neutrons that interact with the iron dump. We find that neutron-initiated bremsstrahlung contributions are comparable to proton-initiated ones, in terms of the resulting flux and the range of couplings that can be probed. The neutron bremsstrahlung can be used to probe dark gauge bosons with non-zero neutron coupling. In particular, we investigate protophobic gauge bosons and find that FASER/FASER2 can probe new parameter space. We also illustrate the possibility of neutron-induced secondary particles by considering axion-like particles with electron couplings. We conclude that the physics potential of FASER/FASER2 in terms of new physics searches can be greatly extended and improved with the inclusion of neutron interactions.

Introduction – Light (sub-GeV) new physics particles feebly interacting with Standard Model (SM) particles are receiving increasing attention [1] as they can address various phenomenological issues including experimental anomalies, e.g., LSND [2], MiniBooNE [3–5], muon $g-2$ [6–8], and ATOMKI [9–13] anomalies. In particular, portal scenarios in connection to low-mass dark matter strongly motivate sub-GeV-range bosonic mediators of this sort [14]. Due to their feebly-interacting nature and low-mass scale, accelerator-based experiments utilizing high-intensity particle beams, i.e., beam-dump-type or fixed-target experiments, are better suited than high-energy colliders in their searches. These intensity-frontier experiments conventionally use incident beam particles (e.g., protons and electrons) and neutral mesons (e.g., π^0 , η , η') as the sources for producing the above-mentioned light dark-sector mediators. Recent studies pointed out the use of charged mesons (e.g. π^\pm , K^\pm) [15–18] and secondary photons and electrons [19, 20] as well. The large beam intensity essentially allows for copious production of such source particles, hence the mediators can be produced abundantly.

In this Letter, we point out that *neutrons* can serve as a new promising route, mostly overlooked thus far, to search for new physics signatures in beam-dump experiments. It has been standard lore that neutrons are a nuisance, as they induce unwanted backgrounds, especially in short-baseline experiments. However, putting

aside the fact that neutrons are electromagnetically neutral, they are as rich in hadronic properties as protons. Therefore, they are (almost) equally capable of inducing new physics as well as SM particles; this new production channel allows us to explore a new set of models, in particular protophobic ones, at dump facilities and provide information complementary to existing searches.

A variety of experiments can make use of neutrons to search for beyond the SM (BSM) particles. Examples include forward physics facilities (FPFs) [21] such as FASER [22], FLArE [23], SND@LHC [24], FORMOSA [25], and stopped-pion neutrino experiments like KARMEN [26, 27], CCM [20, 28], COHERENT [29], and JSNS² [30]. While experiments using lower-energy particle beams would provide interesting opportunities, here we focus on the FASER/FASER2 setup as they are characterized by features distinctive from others.

The ongoing FASER experiment is a part of the FPF program, which aims to explore BSM physics at high energies in a unique way [21]. It seeks signals coming from the interaction point (IP) at ATLAS on the LHC beam line. Figure 1 (not to scale) schematically depicts its experimental setup as well as possible BSM sources. Existing studies which discuss searches for new light scalars [31–33], heavy neutral leptons [34], axion-like particles (ALPs) [35, 36], and dark gauge bosons [37–41] employ (short-lived) mesons, which decay before the LHC magnets, and photons, which survive beyond them. We note that a large number of neutrons are also produced at the IP and, undeflected by the magnets due to their electrically neutral nature, are dumped to TAN/TAXN. Originating from the LHC proton-proton collisions, such neutrons are as energetic as $\mathcal{O}(\text{TeV})$, and inside TAN/TAXN they can result in secondary particles carrying large enough energy to produce BSM particles. This scheme

* bdev@wustl.edu

† dutta@tamu.edu

‡ than@pitt.edu

§ aparaajitha_96@tamu.edu

¶ doojin.kim@tamu.edu

** hyunyong@cern.ch

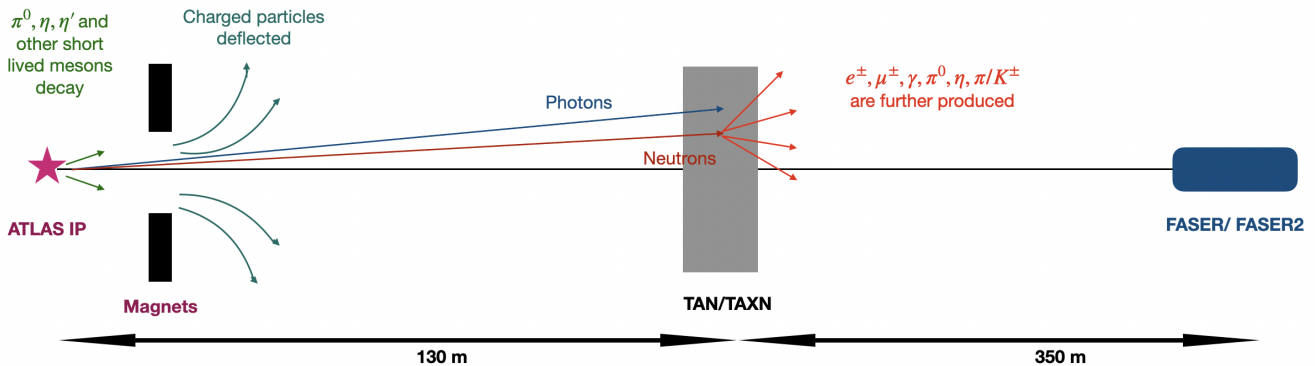


Figure 1: A schematic depiction of our main idea, taking the FASER/FASER2 setup as an example. Short-lived mesons and hadrons produced at the ATLAS IP decay before the magnets placed at 20 m which deflect away the charged particles. Neutrons and photons are collected at the iron dump (TAN/TAXN) 130 m away. The new particles, produced from either neutron bremsstrahlung or secondary emission induced by neutrons at the dump, can be registered at the FASER/FASER2 detector 350 m away.

introduces a new experimental concept, *neutron beam-dump experiments*. In this context, we propose extending the BSM search program of FASER by including this neutron channel. For illustration, we will consider massive vector particles including protophobic gauge bosons that benefit from neutron bremsstrahlung and ALPs interacting with the SM photon and electron that utilize extra photons and electrons/positrons resulting from the neutron beam dump.

Neutron Bremsstrahlung – Neutron bremsstrahlung involves high-energy neutrons radiating particles while interacting (in)elastically with target nuclei. Bremsstrahlung contributions arising in both initial and final states are suppressed due to their destructive interference [42] as modeled by Regge/Pomeron exchanges [43, 44]. The most dominant bremsstrahlung effect is from initial-state radiation (ISR) when a neutron undergoes non-single diffractive (NSD) processes.

As in the proton-initiated bremsstrahlung, the emitted particle is not only forward-directed with respect to the incoming neutron momentum but also carries most of the neutron energy. Thus the differential ISR cross-section $d\sigma_{\text{brem}}$ can be factorized into the NSD cross-section σ_{NSD} and the differential splitting probability dP :

$$d\sigma_{\text{brem}} = \sigma_{\text{NSD}} \cdot dP, \quad (1)$$

where the NSD cross-section is parametrized as $\sigma_{\text{NSD}} = 1.76 + 19.8 (s/\text{GeV}^2)^{0.057}$ mb [45] with s being the center-of-mass energy squared. The splitting probability dP can be expressed in terms of a splitting function that depends on the energy, angle from the incoming neutron, mass, and coupling strength of the gauge boson that is emitted from a neutron with momentum p_n [46]. It also carries information on the off-shell nature of the intermediate neutron as well as the form factor; see Appendix A for details. Using this formulation, we obtain the number of gauge bosons from neutron ISR:

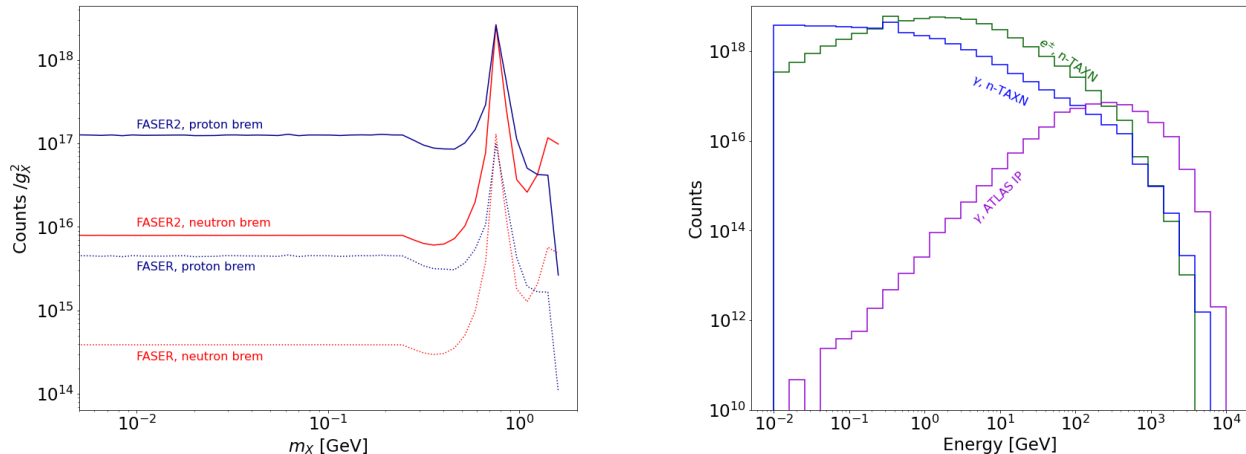
$$dN_{\text{brem}} = N_A \rho_T Z_T \lambda_T d\sigma_{\text{brem}}/A_T, \quad (2)$$

where N_A , ρ_T , Z_T , A_T , and λ_T are the Avogadro's number, density, atomic number, atomic mass, and the mean free path of neutrons in target T, respectively. Since TAN/TAXN is composed of iron, we use $\rho_{\text{Fe}} = 7.874 \text{ g/cm}^3$, $A_{\text{Fe}} = 56$, and $Z_{\text{Fe}} = 26$. For neutron energies greater than 1 GeV, $\lambda_{\text{Fe}} \sim 11.8 \text{ cm}$.

For models such as $U(1)_{B-L}$ [37], secluded $U(1)_X$ [47] and $U(1)_{B-3L_i}$ [38], proton bremsstrahlung has been considered to be a dominant source of high-energy new gauge bosons. The neutron bremsstrahlung, as sketched above, can contribute extensively to the production of gauge bosons especially with neutron couplings. Figure 2a depicts the flux of gauge bosons X arising from neutron bremsstrahlung (red lines) in comparison to those from proton bremsstrahlung (blue lines) for the same normalized coupling. Although the center-of-mass energy of the neutron-target collision ($\sqrt{s} \sim 40 \text{ GeV}$ for a 1 TeV neutron) is much less than that of a proton-proton collision ($\sqrt{s} = 14 \text{ TeV}$), the large number of available targets within a mean free path at the dump enhances neutron bremsstrahlung. This, along with the difference in form factor structures, results in an $\mathcal{O}(10)$ difference in the proton versus neutron-induced flux.

Particles from neutrons-on-target – Neutrons undergoing inelastic interactions with the iron dump at TAN/TAXN produce a large flux of SM particles including photons, charged leptons, and charged and neutral mesons. This provides an opportunity to probe BSM physics via long-lived (boosted decay lengths greater than 20 m) or stable charged particles such as e^\pm , μ^\pm , π^\pm , etc, which are unavailable at the LHC pp collision because they are bent away by the magnets. We estimate the fluxes of these particles by neutrons-on-TAN/TAXN simulations done with GEANT4 [48] for which we use the injection neutron energy spectrum available in EPOSLHC [49] and made available in the FORESEE package [50].

Figure 2b depicts the fluxes of electrons, positrons, and photons that are produced by neutrons on TAXN and are directed towards FASER2 (similar features exist at TAN for FASER). When compared to the photon flux created



(a) Fluxes of light gauge bosons from proton (blue) and neutron (red) bremsstrahlung towards FASER (dotted) and FASER2 (solid).

(b) Fluxes of particles towards FASER2: photons from IP (violet) and neutron-TAXN interactions (blue) and e^\pm from neutron-TAXN interactions (green).

Figure 2: Particles from neutron-TAXN interactions, (a) gauge bosons from neutron bremsstrahlung, and (b) secondary particles towards FASER2. FASER plots are normalized to a luminosity of 150 fb^{-1} and FASER2 to 3 ab^{-1} .

at the IP, we observe that the neutrons induce a larger but softer flux at the TAN/TAXN. More quantitatively, the total number of photons induced by these interactions is ~ 10 times larger than those from the IP. We will see that this large flux helps improve the FASER/FASER2 sensitivity of ALPs.

New gauge bosons from neutron bremsstrahlung

– We first consider a new light gauge boson (X) of mass m_X , coupling to both protons and neutrons, as well as to charged leptons and neutrinos, with strength g_X and charges x_f :

$$\mathcal{L}_{\text{gauge}} \supset \frac{1}{2} m_X^2 X_\mu X^\mu - g_X \sum_f x_f \bar{f} \gamma^\mu f X_\mu. \quad (3)$$

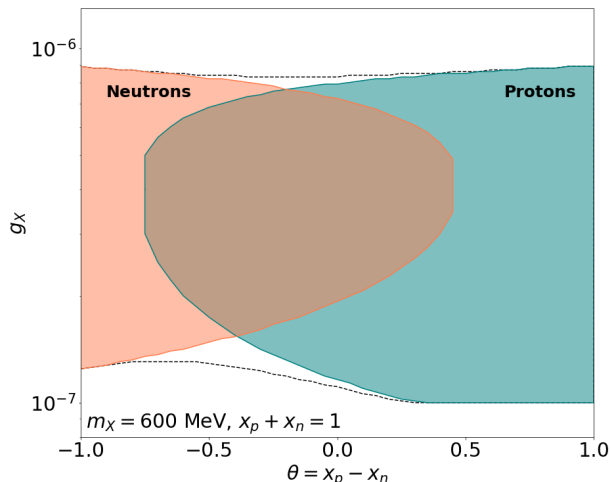
We present the sensitivity estimates at FASER/FASER2 based on a negligible background assumption [36], hence we show the contours for 3 events, which is the upper limit of the 95% confidence level (CL). Figure 3a demonstrates the expected sensitivity of FASER2 for an example where $x_p + x_n = 1$, $x_e = -1$, and $x_{\nu_e} = 0$. Defining a variable $\theta = x_p - x_n$, we plot the range of couplings that can be probed by proton and/or neutron bremsstrahlung for θ values from -1 (protophobic limit) to 1 (neutrophobic limit) for a fixed $m_X = 600 \text{ MeV}$. Thus, the strength of couplings that can be probed through neutron bremsstrahlung is of the same order as that which can be probed through proton bremsstrahlung. The black dotted line is the combined sensitivity from both proton and neutron bremsstrahlung contributions. This shows that both contributions must be included for models where both couplings are relevant, such as when $\theta = 0$ [as in the $U(1)_{B-L}$ model]. Therefore, at FASER2, neutron bremsstrahlung can provide additional sensitivity for

gauge boson models that contain neutron couplings. The protophobic case and simulation details are explained in Appendices B and C, respectively.

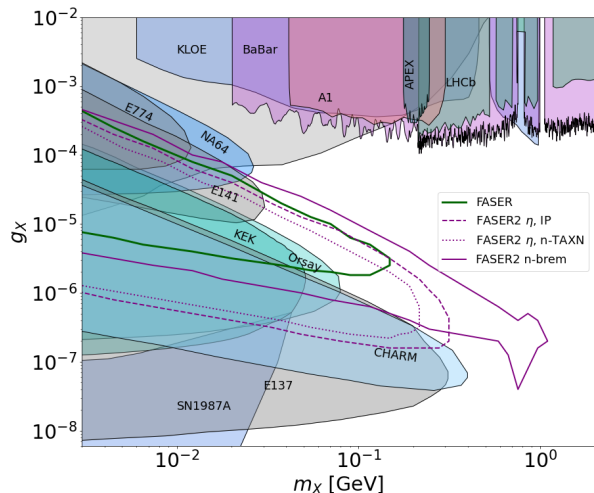
We now focus on the protophobic case, $\theta = -1$, and look at the FASER sensitivity for different gauge boson masses. In this case, the charge $x_f = B_f - Q_f$, where B_f is the baryon number and Q_f is the electric charge. In other words, the gauge boson couples to up-type (u) and down-type (d) quarks with charges $x_u = -1/3$ and $x_d = 2/3$ respectively, while for charged leptons, $x_l = -1$ [51]. This particular choice of couplings does not make the model anomaly-free with SM particles only. However, the anomaly can be evaded by introducing additional matter content to the model [52, 53]. We note that protophobic gauge bosons with $m_X \sim 17 \text{ MeV}$ were invoked, for instance, to explain the ATOMKI anomaly [54–56], but now this explanation seems to be disfavored by neutrino [57] and pion decay [58] constraints.

It is important to note that lighter gauge bosons ($m_X \lesssim 500 \text{ MeV}$) can appear from neutral meson decays as well. For this particular choice of quark couplings, the protophobic gauge boson does not directly couple to π^0 , but it couples to η and η' mesons. At FASER, we observe that the fluxes from η decay and neutron bremsstrahlung dominate over that from η' decay. We use the meson fluxes generated by EPOSLHC [49] and made available in the FORESEE package [50]. To check the uncertainty on the fluxes, we compared the fluxes of η , η' , and neutrons generated by EPOSLHC and QSCJET, but found them to be very similar.

Figure 3b shows the 95% CL sensitivity in the gauge boson mass-coupling plane at FASER (green) and FASER2 (purple). We find that the high-energy η and neutrons at FASER facilitate searches for protophobic



(a) Comparison of FASER sensitivities to neutron (pink) and proton (teal) bremsstrahlung for different $U(1)$ charges with a fixed $m_X = 600$ MeV. The dotted curve shows the total sensitivity.



(b) FASER (green) and FASER2 (purple) sensitivities for protophobic gauge bosons ($\theta = -1$). The purple FASER2 curves are broken down for various sources. The shaded regions show the current exclusion.

Figure 3: FASER/FASER2 sensitivities for neutron-induced signal of protophobic gauge bosons.

gauge bosons in a region that has not been previously explored by beam-dump and other experiments (shaded regions, taken from Ref. [51]). The sensitivity will be further improved at FASER2 with higher luminosity. The different contributions to FASER2 are broken down to show that neutron bremsstrahlung (solid) plays a vital role in probing the middle-right region of parameter space (short lifetimes) for all masses. The reason is that neutron-induced gauge bosons are produced at TAN/TAXN, not at IP, i.e., closer to the detector, and are more energetic. The “beak” shape at the high-mass edge corresponds to the peak in the bremsstrahlung flux in Figure 2a at $m_X \simeq 780$ MeV, which is due to the ρ meson resonance.

We also include the protophobic gauge bosons that appear from the decay of η meson decays as shown by the dashed and dotted purple lines, corresponding to the η mesons produced at the IP (from pp collisions) and at TAXN (from neutron interactions with the dump), respectively. Although gauge bosons appearing from these decays are the most dominant for $m_X < m_\eta = 540$ MeV, they only probe parameters that have already been excluded by electron beam-dump experiments. Therefore, we realize that protophobic gauge bosons from neutron bremsstrahlung give us the most insight.

For comparison, we also show the existing experimental constraints on the protophobic gauge boson model by the shaded regions, taken from Ref. [51], except for the supernova limit, which was adapted from Ref. [59]. The grey bounds shown in the plot arise from Υ [60, 61] and η decays [62, 63], from longitudinal enhancements [64, 65], in $B_{u,d} \rightarrow KX$ decays [66], $K \rightarrow \pi X$ [67, 68], $Z \rightarrow X\gamma$ [69, 70], and the observational lack of new anomaly-

canceling fermions [64, 71, 72]. The electron beam-dump constraints come from KEK [73], E137 [74], E141 [75], E774 [76], NA64 [77], and Orsay [78]), while the proton beam-dump constraints are from CHARM [79]. The e^+e^- collider constraints from BaBar [80] and KLOE [81], pp collider constraint from LHCb [82] and others such as A1 [83] and APEX [84] are also depicted in the sensitivity plot.

ALPs with neutron dump – ALPs with couplings to photons have been studied at FASER [35, 36], where high-energy photons produced at the IP convert to ALPs through the Primakoff scattering at the TAN/TAXN. These ALPs, which are very energetic with momentum $\mathcal{O}(1$ TeV), allow FASER to explore new parameter space toward the middle-right region beyond the existing beam-dump constraints.

While the FASER sensitivity to ALPs interacting with SM fermions has been studied using heavy meson decays and Yukawa-like coupling structure [21], ALPs with electron couplings have received less attention. We emphasize that there are plenty of electrons and positrons created at the TAN/TAXN due to neutron interactions. As we show here, these can be utilized to study ALPs with electron couplings at FASER. In addition, low-energy photons produced at the TAN/TAXN facilitate Compton-like scattering processes, hence serving as a factory of electrophilic ALPs. With a denoting the ALP field, the relevant Lagrangian for the ALPs is

$$\mathcal{L}_{ae} \supset -\frac{1}{2}m_a^2 a^2 - ig_{ae} a \bar{e} \gamma^5 e, \quad (4)$$

from which we identify three major production channels: i) Compton-like scattering ($\gamma e^- \rightarrow a e^-$) [85], ii) associ-

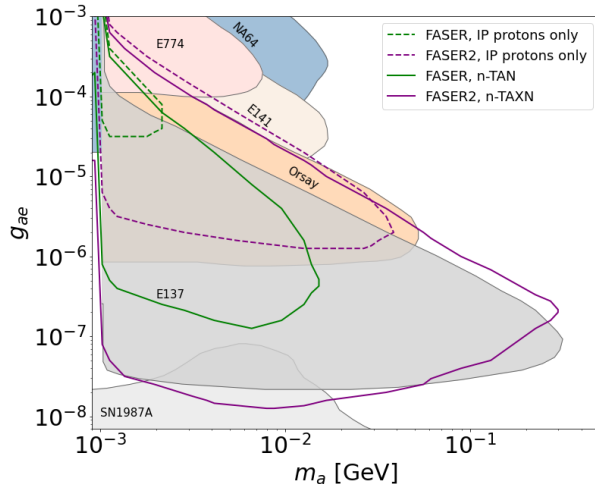


Figure 4: Sensitivity of electrophilic ALPs at FASER (green) and FASER2 (purple). The dotted curves correspond to ALPs produced from photons at the IP, whereas the solid curves are from photons, electrons, and positrons produced at the neutron-TAN/TAXN. The shaded regions show the current exclusion [20, 87].

ated production ($e^+e^- \rightarrow a\gamma$), and iii) electron-positron annihilation ($e^+e^- \rightarrow a$) [20, 86]. These ALPs are primarily detected when they decay to electron-positron pairs. Kinematically, only those ALPs heavier than $2m_e \simeq 1$ MeV can decay to e^+e^- pair.

Figure 4 exhibits our sensitivity estimates for these ALPs where the dotted lines are sensitivities only with ALPs produced by IP-origin photons, whereas the solid lines are those produced from secondary photons, electrons, and positrons induced by neutron interactions. The green (purple) lines are for FASER (FASER2). We find that the latter sensitivities are significantly better due to the low-energy photons as well as the additional flux of electrons and positrons. The existing constraints on the ALP parameter space are shown by the shaded regions, where the dominant limits come from previous beam-dump experiments, collected in Ref. [87]. These include E137 [74, 88], Orsay [89], E141 [75], E774 [76], and NA64 [90]. The supernova bound was taken from Ref. [91].

Thus we see that neutron-on-target interactions have a large impact on ALPs with electron couplings. In particular, FASER2 can probe the regions of parameter space ($m_a \sim 100$ MeV, $g_{ae} \sim 10^{-6}$) that are challenging to probe at other lower-energy beam-dump facilities. Here we have used a 30 MeV energy threshold [92] for the e^+e^- final states. For higher energy thresholds (up to several GeVs) [37, 93], we notice that the upper-right region of the sensitivity plot remains unaffected and only the bottom region retracts into the beam-dump exclusion.

Conclusion – This Letter demonstrates with two examples how neutrons can be used for the first time for probing new physics at a high-energy dump facility like

FASER. The high-energy high-intensity neutrons, produced copiously at the proton-proton interaction point escape undeflected by the LHC magnetic field and interact with an iron dump resulting in the bremsstrahlung of new light particles. We derived the FASER2 sensitivity for protophobic gauge bosons, which extends up to ~ 1 GeV in the gauge boson mass when neutron bremsstrahlung is considered. Although we demonstrate this effect in the protophobic scenario, neutrons can provide an additional handle for any model where the new particles have non-zero neutron coupling. Furthermore, since charged particles produced at the IP are deflected by the magnetic field, neutron-induced secondary particles (such as photons and electrons) at the dump allow us to probe BSM particles with couplings to these secondary particles. Utilizing the secondary electrons and positrons, we showed that FASER2 can probe new parameter space for ALP couplings with electrons in the range of $10^{-8} - 10^{-6}$, and mass as heavy as 100 MeV. We also see that neutron-induced photons are much larger in flux as compared to those from the ATLAS IP. While we include their influence on ALPs with electron couplings in this study, we reserve the impact of secondary productions on various other light mediators, such as ALPs with photon couplings, leptophilic scalars, etc. for future work.

Acknowledgments – We thank Brian Batell and Joshua Berger for useful discussions. The work of PSBD is supported in part by the U.S. Department of Energy under Grant No. DE-SC0017987. The work of BD, AK, DK, and HK is supported in part by the U.S. Department of Energy Grant DE-SC0010813. The work of TH is supported in part by the U.S. Department of Energy under grant No. DE-SC0007914 and by the PITT PACC.

Appendix A: Neutron Bremsstrahlung

The ISR probability from neutrons, under the assumption that the gauge boson is highly forward and energetic, is given by [46]

$$dP = \omega_V(g_X, m_X, z, p_T^2) \cdot J\left(\frac{z, p_T^2}{E_X, \cos\theta_X}\right) dE_X d\cos\theta_X, \quad (\text{A1})$$

where E_X , θ_X , m_X , and g_X are the energy, angle with respect to the incoming neutron, mass, and coupling strength of the gauge boson that is radiated from a neutron with momentum p_n and mass m_n . We introduce p_T , the transverse momentum of the gauge boson, and z , the fraction of longitudinal momentum carried by the vector boson:

$$p_T = p_X \sin\theta, \quad z = \frac{p_X \cos\theta_X}{p_n}. \quad (\text{A2})$$

$\omega_V(z, p_T^2)$ is the splitting function of the gauge boson, which can be expressed as

$$\omega_V(z, p_T^2) = \frac{g_X^2}{8\pi^2} |F_X^n(m_X^2, m_n^2 - H/z)|^2 \times \frac{1}{H} \left[z - z(1-z) \left(\frac{2m_n^2 + m_X^2}{H} \right) + \frac{H}{2zm_X^2} \right], \quad (\text{A3})$$

where H is a measure of how off-shell the intermediate neutron is:

$$H = z[m_n^2 - (p_n - p_X)^2]. \quad (\text{A4})$$

In order to convert the probability into a function of E_V and $\cos\theta_V$, we include the following Jacobian in the differential probability (A1):

$$J\left(\frac{z, p_T^2}{E_X, \cos\theta_X}\right) = \frac{2p_X E_X}{p_n}. \quad (\text{A5})$$

The neutron form factor F_X^n in Eq. (A3) is a product of the timelike form factor $F_{1,X}^n(p_X^2)$ and the hadronic form factor $F_{nn^*,X}(p_{n^*}^2)$, where $p_{n^*} = p_n - p_X$. The timelike form factor is obtained from the Vector Meson Dominance model [94–96] where we express X as a superposition of the isovector and isoscalar mesons ρ and ω :

$$F_{1,X}^n(p_X^2) = \sum_{\omega} \frac{f_{\omega} m_{\omega}^2}{m_{\omega}^2 - p_X^2 - im_{\omega}\Gamma_{\omega}} - \sum_{\rho} \frac{f_{\rho} m_{\rho}^2}{m_{\rho}^2 - p_X^2 - im_{\rho}\Gamma_{\rho}}, \quad (\text{A6})$$

where the sum is over the three different ρ and ω mesons [97], and f_{ω} and f_{ρ} are $\{1.011, -0.881, 0.369\}$ and $\{0.616, 0.223, -0.339\}$, respectively [96]. Note that the neutron form factor is different from the proton form factor due to the relative negative sign between ρ and ω resonances in Eq. (A6).

The hadronic form factor $F_{nn^*,X}(p_{n^*}^2)$ accounts for the off-shell nature of the intermediate neutron [98–105]. Following Refs. [46, 99], we write the hadronic form factor as

$$F_{nn^*,X}(p_{n^*}^2) = \frac{\Lambda_n^4}{\Lambda_n^4 + (p_{n^*}^2 - m_n^2)^2}. \quad (\text{A7})$$

It does not depend strongly on the choice of the cut-off scale Λ_n , which must be chosen to be larger than the mass of the neutron. We choose $\Lambda_n = 1.5$ GeV, similar to that chosen in the proton bremsstrahlung case [46]. This behaves like a momentum cut-off for the off-shell neutron, as the form factor is maximized ($= 1$) when the off-shell nature of the intermediate neutron (encapsulated by $p_{n^*}^2 - m_n^2$) is much less than Λ_n .

Appendix B: Protophobic Gauge Bosons from Meson Decays

Protophobic gauge bosons can be produced directly from neutral meson decays, as they have quark couplings. The branching ratio (BR) of a neutral meson

decay $\mathbf{m} \rightarrow \gamma X$ can be written as

$$\text{BR}(\mathbf{m} \rightarrow \gamma X) = 2 \text{BR}(\mathbf{m} \rightarrow \gamma\gamma) \beta_{\mathbf{m}} \left(\frac{g_X}{e}\right)^2 \left(1 - \frac{m_X^2}{m_{\mathbf{m}}^2}\right)^3, \quad (\text{B1})$$

where $\beta_{\mathbf{m}}$ is the ratio between the photon and X boson couplings of quarks in the meson \mathbf{m} . The only relevant neutral mesons in the SM with a non-negligible BR to two photons are π^0, η and η' [97].

Since the neutral pion is composed of u and d quarks such that $\pi^0 = (u\bar{u} - d\bar{d})/\sqrt{2}$, we observe that β_{π^0} is proportional to $(Q_u x_u - Q_d x_d)^2$. For the protophobic choice of charges $x_f = B_f - Q_f$, we see that $(Q_u x_u - Q_d x_d)^2 = 0$. Therefore, the decay $\pi^0 \rightarrow \gamma X$ does not occur at the tree level.

On the other hand, the η and η' mesons are linear superpositions of the octet meson η_8 and the singlet meson η_0 , with the following quark content:

$$\begin{aligned} \eta_8 &= \frac{1}{\sqrt{6}}(u\bar{u} + d\bar{d} - 2s\bar{s}), \\ \eta_0 &= \frac{1}{\sqrt{3}}(u\bar{u} + d\bar{d} + s\bar{s}). \end{aligned} \quad (\text{B2})$$

We then have

$$\begin{aligned} \eta &= \cos\theta_p \eta_8 - \sin\theta_p \eta_0, \\ \eta' &= \sin\theta_p \eta_8 + \cos\theta_p \eta_0, \end{aligned} \quad (\text{B3})$$

where the mixing angle θ_p lies between -17° and -20° [106]. We take the average value of $\theta_p = -18.5^\circ$ for our numerical analysis but checked that any value within the uncertainty band essentially gives the same result.

Using this value of θ_p , the factors β_{η} and $\beta_{\eta'}$ in Eq. (B1) can be evaluated as

$$\beta_{\eta} = \frac{\phi_{\eta}(X, \gamma)}{\phi_{\eta}(\gamma, \gamma)} = 0.29, \quad (\text{B4})$$

$$\beta_{\eta'} = \frac{\phi_{\eta'}(X, \gamma)}{\phi_{\eta'}(\gamma, \gamma)} = 1.20, \quad (\text{B5})$$

where the functions ϕ can be expressed as

$$\begin{aligned} \phi_{\eta}(V_1, V_2) &= \left[\frac{1}{f_8} \cos\theta_p (x_1^u x_2^u + x_1^d x_2^d - 2x_1^s x_2^s) \right. \\ &\quad \left. - \frac{\sqrt{2}}{f_0} \sin\theta_p (x_1^u x_2^u + x_1^d x_2^d + x_1^s x_2^s) \right]^2 \end{aligned} \quad (\text{B6})$$

$$\begin{aligned} \phi_{\eta'}(V_1, V_2) &= \left[\frac{1}{f_8} \sin\theta_p (x_1^u x_2^u + x_1^d x_2^d - 2x_1^s x_2^s) \right. \\ &\quad \left. + \frac{\sqrt{2}}{f_0} \cos\theta_p (x_1^u x_2^u + x_1^d x_2^d + x_1^s x_2^s) \right]^2 \end{aligned} \quad (\text{B7})$$

Here $f_0 = 1.05 f_{\pi}$ and $f_8 = 1.3 f_{\pi}$ [107], with f_{π} being the pion decay constant [97]. Also, x_i^q is the charge carried by quark $q = u, d, s$ with the gauge boson V_i (where $i = 1, 2$ for X and γ), i.e. $x_X^q \equiv x_q Q_q$ and $x_{\gamma}^q \equiv Q_q$. Therefore,

the branching ratios of $\eta/\eta' \rightarrow X\gamma$ are given by

$$\begin{aligned} \text{BR}(\eta \rightarrow X\gamma) &= 2 \times 0.39 \times 0.29 \left(\frac{g_X}{e}\right)^2 \left(1 - \frac{m_X^2}{m_\eta^2}\right)^3, \\ \text{BR}(\eta' \rightarrow X\gamma) &= 2 \times 0.02 \times 1.20 \left(\frac{g_X}{e}\right)^2 \left(1 - \frac{m_X^2}{m_{\eta'}^2}\right)^3, \end{aligned} \tag{B8}$$

using the fact that $\text{BR}(\eta \rightarrow \gamma\gamma) = 0.39$ and $\text{BR}(\eta' \rightarrow \gamma\gamma) = 0.02$ in the SM [97]. This implies that the η decay contribution to the protophobic gauge boson production is about 5 times stronger than that from the η' decay. This, together with the fact that the η production rate is ~ 9 times higher than that of η' , implies that it is okay to drop the η' contribution from our sensitivity analysis shown in Figure 3.

Appendix C: Simulation Scheme

In order to simulate the gauge bosons from two-body meson decays for a particular gauge boson mass, we utilize the branching ratio in Eq. (B8) as a weight factor for each gauge boson. To simulate event kinematics, we first work in the rest frame of the decaying η meson where the

final state energies are fixed, and the angular distribution is uniform. We construct the four-momentum of X in the rest frame by randomly choosing $\cos\theta$ and ϕ , where θ and ϕ are the polar and azimuthal angles respectively, and then boost it to the laboratory frame to generate events.

Simulating gauge bosons from neutron bremsstrahlung is more involved. Although Eq. (2) gives the number of bremsstrahlung products, all the information about energies and angles of the gauge boson is encapsulated in Eq. (A1). Therefore, we simulate gauge bosons from the latter equation and then normalize it to the former one. Since this probability is under the assumption that the gauge bosons are highly forward-going and energetic, the probability function is highly peaked at $\cos\theta_X = 1$. In order to numerically integrate over $\cos\theta_X$, we pick only the peak value and integrate $\cos\theta_X$ over the angular acceptance of the detector, i.e., if θ_n is the polar angle of the neutron and θ_d is the angle subtended by the detector at the point where the neutron radiates X , the limits of the integral are $\cos(\theta_d - \theta_n) < \cos\theta_X < 1$. For the energy integral, the distribution is not highly-peaked at a specific value. Rather, we find that to a good approximation it linearly increases with E_X for high energies. To select the energies of these radiated bosons for a given neutron energy E_n , we pick E_X from a linear distribution ranging from $E_n/2$ to E_n based on the above assumptions.

-
- [1] P. Agrawal *et al.*, *Eur. Phys. J. C* **81**, 1015 (2021), [arXiv:2102.12143 \[hep-ph\]](#).
- [2] A. Aguilar *et al.* (LSND), *Phys. Rev. D* **64**, 112007 (2001), [arXiv:hep-ex/0104049](#).
- [3] A. A. Aguilar-Arevalo *et al.* (MiniBooNE), *Phys. Rev. Lett.* **102**, 101802 (2009), [arXiv:0812.2243 \[hep-ex\]](#).
- [4] A. A. Aguilar-Arevalo *et al.* (MiniBooNE), *Phys. Rev. Lett.* **121**, 221801 (2018), [arXiv:1805.12028 \[hep-ex\]](#).
- [5] A. A. Aguilar-Arevalo *et al.* (MiniBooNE), *Phys. Rev. D* **103**, 052002 (2021), [arXiv:2006.16883 \[hep-ex\]](#).
- [6] G. W. Bennett *et al.* (Muon g-2), *Phys. Rev. D* **73**, 072003 (2006), [arXiv:hep-ex/0602035](#).
- [7] B. Abi *et al.* (Muon g-2), *Phys. Rev. Lett.* **126**, 141801 (2021), [arXiv:2104.03281 \[hep-ex\]](#).
- [8] D. P. Aguillard *et al.* (Muon g-2), *Phys. Rev. Lett.* **131**, 161802 (2023), [arXiv:2308.06230 \[hep-ex\]](#).
- [9] A. J. Krasznahorkay *et al.*, *Phys. Rev. Lett.* **116**, 042501 (2016), [arXiv:1504.01527 \[nucl-ex\]](#).
- [10] A. J. Krasznahorkay *et al.*, (2019), [arXiv:1910.10459 \[nucl-ex\]](#).
- [11] A. J. Krasznahorkay, M. Csatlós, L. Csige, J. Gulyás, A. Krasznahorkay, B. M. Nyakó, I. Rajta, J. Timár, I. Vajda, and N. J. Sas, *Phys. Rev. C* **104**, 044003 (2021), [arXiv:2104.10075 \[nucl-ex\]](#).
- [12] A. J. Krasznahorkay *et al.*, *Phys. Rev. C* **106**, L061601 (2022), [arXiv:2209.10795 \[nucl-ex\]](#).
- [13] A. J. Krasznahorkay, A. Krasznahorkay, M. Csatlós, L. Csige, J. Timár, M. Begala, A. Krakó, I. Rajta, and I. Vajda, (2023), [arXiv:2308.06473 \[nucl-ex\]](#).
- [14] B. Batell *et al.*, in *Snowmass 2021* (2022) [arXiv:2207.06898 \[hep-ph\]](#).
- [15] C. Y. Pang, R. H. Hildebrand, G. D. Cable, and R. Stiening, *Phys. Rev. D* **8**, 1989 (1973).
- [16] C. E. Carlson and B. C. Rislow, *Phys. Rev. D* **86**, 035013 (2012), [arXiv:1206.3587 \[hep-ph\]](#).
- [17] B. Dutta, D. Kim, A. Thompson, R. T. Thornton, and R. G. Van de Water, *Phys. Rev. Lett.* **129**, 111803 (2022), [arXiv:2110.11944 \[hep-ph\]](#).
- [18] P. S. B. Dev, B. Dutta, T. Han, and D. Kim, (2023), [arXiv:2304.02031 \[hep-ph\]](#).
- [19] F. Capozzi, B. Dutta, G. Gurung, W. Jang, I. M. Shoemaker, A. Thompson, and J. Yu, *Phys. Rev. D* **108**, 075019 (2023), [arXiv:2307.03878 \[hep-ph\]](#).
- [20] A. A. Aguilar-Arevalo *et al.* (CCM), *Phys. Rev. D* **107**, 095036 (2023), [arXiv:2112.09979 \[hep-ph\]](#).
- [21] J. L. Feng *et al.*, *J. Phys. G* **50**, 030501 (2023), [arXiv:2203.05090 \[hep-ex\]](#).
- [22] A. Ariga *et al.* (FASER), (2018), [arXiv:1812.09139 \[physics.ins-det\]](#).
- [23] B. Batell, J. L. Feng, and S. Trojanowski, *Phys. Rev. D* **103**, 075023 (2021), [arXiv:2101.10338 \[hep-ph\]](#).
- [24] C. Ahdida *et al.* (SHiP), (2020), [arXiv:2002.08722 \[physics.ins-det\]](#).
- [25] S. Foroughi-Abari, F. Kling, and Y.-D. Tsai, *Phys. Rev. D* **104**, 035014 (2021), [arXiv:2010.07941 \[hep-ph\]](#).
- [26] G. Drexlin *et al.* (KARMEN), *Phys. Lett. B* **267**, 321 (1991).
- [27] J. Kleinfeller (KARMEN), in *29th Rencontres de Moriond: Particle Astrophysics: Perspectives in Particle Physics, Atomic Physics and Gravitation* (1994) pp. 245–249.
- [28] A. A. Aguilar-Arevalo *et al.*, (2023), [arXiv:2309.02599 \[hep-ph\]](#).
- [29] D. Akimov *et al.*, in *Snowmass 2021* (2022)

- arXiv:2204.04575 [hep-ex].
- [30] S. Ajimura *et al.*, (2017), arXiv:1705.08629 [physics.ins-det].
- [31] J. L. Feng, I. Galon, F. Kling, and S. Trojanowski, *Phys. Rev. D* **97**, 055034 (2018), arXiv:1710.09387 [hep-ph].
- [32] K. J. Kelly, F. Kling, D. Tuckler, and Y. Zhang, *Phys. Rev. D* **105**, 075026 (2022), arXiv:2111.05868 [hep-ph].
- [33] F. Kling, S. Li, H. Song, S. Su, and W. Su, *JHEP* **08**, 001 (2023), arXiv:2212.06186 [hep-ph].
- [34] F. Kling and S. Trojanowski, *Phys. Rev. D* **97**, 095016 (2018), arXiv:1801.08947 [hep-ph].
- [35] F. Kling and P. Quilés, *Phys. Rev. D* **106**, 055036 (2022), arXiv:2204.03599 [hep-ph].
- [36] J. L. Feng, I. Galon, F. Kling, and S. Trojanowski, *Phys. Rev. D* **98**, 055021 (2018), arXiv:1806.02348 [hep-ph].
- [37] A. Ariga *et al.* (FASER), *Phys. Rev. D* **99**, 095011 (2019), arXiv:1811.12522 [hep-ph].
- [38] F. Kling, *Phys. Rev. D* **102**, 015007 (2020), arXiv:2005.03594 [hep-ph].
- [39] T. Araki, K. Asai, H. Otono, T. Shimomura, and Y. Takubo, *JHEP* **03**, 072 (2021), [Erratum: *JHEP* 06, 087 (2021)], arXiv:2008.12765 [hep-ph].
- [40] B. Batell, J. L. Feng, M. Fieg, A. Ismail, F. Kling, R. M. Abraham, and S. Trojanowski, *Phys. Rev. D* **105**, 075001 (2022), arXiv:2111.10343 [hep-ph].
- [41] H. Abreu *et al.* (FASER), (2023), arXiv:2308.05587 [hep-ex].
- [42] P. Lebiedowicz and A. Szczurek, *Phys. Rev. D* **87**, 114013 (2013), arXiv:1302.4346 [hep-ph].
- [43] A. Donnachie and P. V. Landshoff, *Phys. Lett. B* **123**, 345 (1983).
- [44] A. Donnachie and P. V. Landshoff, *Nucl. Phys. B* **244**, 322 (1984).
- [45] A. K. Likhoded, A. V. Luchinsky, and A. A. Novoselov, *Phys. Rev. D* **82**, 114006 (2010), arXiv:1005.1827 [hep-ph].
- [46] S. Foroughi-Abari and A. Ritz, *Phys. Rev. D* **105**, 095045 (2022), arXiv:2108.05900 [hep-ph].
- [47] K. Jodowski, F. Kling, L. Roszkowski, and S. Trojanowski, *Phys. Rev. D* **101**, 095020 (2020), arXiv:1911.11346 [hep-ph].
- [48] S. Agostinelli *et al.* (GEANT4), *Nucl. Instrum. Meth. A* **506**, 250 (2003).
- [49] T. Pierog, I. Karpenko, J. M. Katzy, E. Yatsenko, and K. Werner, *Phys. Rev. C* **92**, 034906 (2015), arXiv:1306.0121 [hep-ph].
- [50] F. Kling and S. Trojanowski, *Phys. Rev. D* **104**, 035012 (2021), arXiv:2105.07077 [hep-ph].
- [51] P. Ilten, Y. Soreq, M. Williams, and W. Xue, *JHEP* **06**, 004 (2018), arXiv:1801.04847 [hep-ph].
- [52] P. Fileviez Perez and M. B. Wise, *Phys. Rev. D* **82**, 011901 (2010), [Erratum: *Phys.Rev.D* 82, 079901 (2010)], arXiv:1002.1754 [hep-ph].
- [53] T. R. Dulaney, P. Fileviez Perez, and M. B. Wise, *Phys. Rev. D* **83**, 023520 (2011), arXiv:1005.0617 [hep-ph].
- [54] J. L. Feng, B. Fornal, I. Galon, S. Gardner, J. Smolinsky, T. M. P. Tait, and P. Tanedo, *Phys. Rev. Lett.* **117**, 071803 (2016), arXiv:1604.07411 [hep-ph].
- [55] J. L. Feng, B. Fornal, I. Galon, S. Gardner, J. Smolinsky, T. M. P. Tait, and P. Tanedo, *Phys. Rev. D* **95**, 035017 (2017), arXiv:1608.03591 [hep-ph].
- [56] J. L. Feng, T. M. P. Tait, and C. B. Verhaaren, *Phys. Rev. D* **102**, 036016 (2020), arXiv:2006.01151 [hep-ph].
- [57] P. B. Denton and J. Gehrlein, *Phys. Rev. D* **108**, 015009 (2023), arXiv:2304.09877 [hep-ph].
- [58] M. Hostert and M. Pospelov, *Phys. Rev. D* **108**, 055011 (2023), arXiv:2306.15077 [hep-ph].
- [59] E. Rrapaj and S. Reddy, *Phys. Rev. C* **94**, 045805 (2016), arXiv:1511.09136 [nucl-th].
- [60] A. Aranda and C. D. Carone, *Phys. Lett. B* **443**, 352 (1998), arXiv:hep-ph/9809522.
- [61] H. Albrecht *et al.* (ARGUS), *Z. Phys. C* **31**, 181 (1986).
- [62] S. Tulin, *Phys. Rev. D* **89**, 114008 (2014), arXiv:1404.4370 [hep-ph].
- [63] S. Prakhov *et al.*, *Phys. Rev. C* **78**, 015206 (2008).
- [64] J. A. Dror, R. Lasenby, and M. Pospelov, *Phys. Rev. D* **96**, 075036 (2017), arXiv:1707.01503 [hep-ph].
- [65] J. A. Dror, R. Lasenby, and M. Pospelov, *Phys. Rev. Lett.* **119**, 141803 (2017), arXiv:1705.06726 [hep-ph].
- [66] J. Grygier *et al.* (Belle), *Phys. Rev. D* **96**, 091101 (2017), [Addendum: *Phys.Rev.D* 97, 099902 (2018)], arXiv:1702.03224 [hep-ex].
- [67] A. Alavi-Harati *et al.* (KTeV), *Phys. Rev. Lett.* **93**, 021805 (2004), arXiv:hep-ex/0309072.
- [68] A. V. Artamonov *et al.* (E949), *Phys. Rev. Lett.* **101**, 191802 (2008), arXiv:0808.2459 [hep-ex].
- [69] M. Acciari *et al.* (L3), *Phys. Lett. B* **412**, 201 (1997).
- [70] P. Abreu *et al.* (DELPHI), *Z. Phys. C* **74**, 57 (1997), [Erratum: *Z.Phys.C* 75, 580 (1997)].
- [71] J. M. Cline, G. Dupuis, Z. Liu, and W. Xue, *JHEP* **08**, 131 (2014), arXiv:1405.7691 [hep-ph].
- [72] B. A. Dobrescu and C. Frugiuele, *Phys. Rev. Lett.* **113**, 061801 (2014), arXiv:1404.3947 [hep-ph].
- [73] A. Konaka *et al.*, *Phys. Rev. Lett.* **57**, 659 (1986).
- [74] J. D. Bjorken, S. Ecklund, W. R. Nelson, A. Abashian, C. Church, B. Lu, L. W. Mo, T. A. Nunamaker, and P. Rassmann, *Phys. Rev. D* **38**, 3375 (1988).
- [75] E. M. Riordan *et al.*, *Phys. Rev. Lett.* **59**, 755 (1987).
- [76] A. Bross, M. Crisler, S. H. Pordes, J. Volk, S. Errede, and J. Wrbanek, *Phys. Rev. Lett.* **67**, 2942 (1991).
- [77] D. Banerjee *et al.* (NA64), *Phys. Rev. Lett.* **120**, 231802 (2018), arXiv:1803.07748 [hep-ex].
- [78] M. Davier and H. Nguyen Ngoc, *Phys. Lett. B* **229**, 150 (1989).
- [79] F. Bergsma *et al.* (CHARM), *Phys. Lett. B* **157**, 458 (1985).
- [80] J. P. Lees *et al.* (BaBar), *Phys. Rev. Lett.* **113**, 201801 (2014), arXiv:1406.2980 [hep-ex].
- [81] A. Anastasi *et al.* (KLOE-2), *Phys. Lett. B* **757**, 356 (2016), arXiv:1603.06086 [hep-ex].
- [82] R. Aaij *et al.* (LHCb), *Phys. Rev. Lett.* **120**, 061801 (2018), arXiv:1710.02867 [hep-ex].
- [83] H. Merkel *et al.*, *Phys. Rev. Lett.* **112**, 221802 (2014), arXiv:1404.5502 [hep-ex].
- [84] S. Abrahamyan *et al.* (APEX), *Phys. Rev. Lett.* **107**, 191804 (2011), arXiv:1108.2750 [hep-ex].
- [85] D. Aristizabal Sierra, V. De Romeri, L. J. Flores, and D. K. Papoulias, *JHEP* **03**, 294 (2021), arXiv:2010.15712 [hep-ph].
- [86] E. Nardi, C. D. R. Carvajal, A. Ghoshal, D. Meloni, and M. Raggi, *Phys. Rev. D* **97**, 095004 (2018), arXiv:1802.04756 [hep-ph].
- [87] C. O'Hare, "Axionlimits," <https://cajohare.github.io/AxionLimits/> (2020).
- [88] S. Andreas, O. Lebedev, S. Ramos-Sanchez, and A. Ringwald, *JHEP* **08**, 003 (2010), arXiv:1005.3978 [hep-ph].
- [89] D. J. Bechis, T. W. Dombeck, R. W. Ellsworth, E. V. Sager, P. H. Steinberg, L. J. Teig, J. K. Yoh, and R. L. Weitz, *Phys. Rev. Lett.* **42**, 1511 (1979), [Erratum: *Phys.Rev.Lett.* 43, 90 (1979)].
- [90] Y. M. Andreev *et al.*, *Phys. Rev. D* **104**, L091701 (2021),

- arXiv:2108.04195 [hep-ex].
- [91] G. Lucente and P. Carenza, *Phys. Rev. D* **104**, 103007 (2021), arXiv:2107.12393 [hep-ph].
- [92] B. Batell, J. L. Feng, A. Ismail, F. Kling, R. M. Abraham, and S. Trojanowski, *Phys. Rev. D* **104**, 035036 (2021), arXiv:2107.00666 [hep-ph].
- [93] A. Berlin and F. Kling, *Phys. Rev. D* **99**, 015021 (2019), arXiv:1810.01879 [hep-ph].
- [94] E. Tomasi-Gustafsson, F. Lacroix, C. Duterte, and G. I. Gakh, *Eur. Phys. J. A* **24**, 419 (2005), arXiv:nucl-th/0503001.
- [95] A. Faessler, M. I. Krivoruchenko, and B. V. Martemyanov, *Phys. Rev. C* **82**, 038201 (2010), arXiv:0910.5589 [hep-ph].
- [96] C. Adamuščin, E. Bartoš, S. Dubnička, and A. Z. Dubničková, *Phys. Rev. C* **93**, 055208 (2016), arXiv:1601.06190 [hep-ph].
- [97] R. L. Workman and Others (Particle Data Group), *PTEP* **2022**, 083C01 (2022).
- [98] H. Habermann, C. Bennhold, T. Mart, and T. Feuster, *Phys. Rev. C* **58**, R40 (1998), arXiv:nucl-th/9804051.
- [99] T. Feuster and U. Mosel, *Phys. Rev. C* **59**, 460 (1999), arXiv:nucl-th/9803057.
- [100] Y.-s. Oh, A. I. Titov, and T. S. H. Lee, *Phys. Rev. C* **63**, 025201 (2001), arXiv:nucl-th/0006057.
- [101] S. Janssen, J. Ryckebusch, D. Debruyne, and T. Van Cauteren, *Phys. Rev. C* **65**, 015201 (2002), arXiv:nucl-th/0107028.
- [102] G. Penner and U. Mosel, *Phys. Rev. C* **66**, 055211 (2002), arXiv:nucl-th/0207066.
- [103] G. Penner and U. Mosel, *Phys. Rev. C* **66**, 055212 (2002), arXiv:nucl-th/0207069.
- [104] D. Ronchen, M. Doring, F. Huang, H. Habermann, J. Haidenbauer, C. Hanhart, S. Krewald, U. G. Meissner, and K. Nakayama, *Eur. Phys. J. A* **49**, 44 (2013), arXiv:1211.6998 [nucl-th].
- [105] H. Kamano, S. X. Nakamura, T. S. H. Lee, and T. Sato, *Phys. Rev. C* **88**, 035209 (2013), arXiv:1305.4351 [nucl-th].
- [106] R. Escobedo and E. Royo, *Phys. Lett. B* **807**, 135534 (2020), arXiv:2003.08379 [hep-ph].
- [107] B. M. K. Nefkens and J. W. Price, *Phys. Scripta T* **99**, 114 (2002), arXiv:nucl-ex/0202008.